# Knots Arising From the Planar Equal-Mass Collisionless Three-Body Problem

Jasper Sun

## Abstract

We present a series of steps that transform reduced equal-mass collisionless planar three-body configurations into closed curves in $\mathbb{R}^3$. Exploiting a center-of-mass constraint and a size constraint, we reduce the original configuration in $\mathbb{R}^6$ to $\mathbb{R}^4$. We then use a rotation and an additional stereographic projection onto $\mathbb{R}^3$. This procedure turns a periodic orbit into a closed curve that can be classified as a knot. We apply our method to the fifteen periodic configurations presented by Šuvakov and Dmitrašinović in [4] and show that most of these trajectories become the unknot under our projection. However, three orbits become trefoils and one becomes a figure-eight. We discuss the direction of possible future work.

## 1. Introduction

This paper answers two questions:

1. Can we find an orbit in each of the classes listed in the paper of Šuvakov and Dmitrašinović which is non-trivially knotted? No.
2. Can two orbits with the same free group element (for more information about the free group, see [4]) have different knot types? Yes.

The classical three-body problem has been studied by mathematicians and physicists since Newton found the closed-form for the two-body problem. In the 19th century, Poincaré showed that the general three-body problem is non-integrable [3]. Nonetheless, families of periodic orbits have been discovered and studied for their insights into $n$-body systems. The planar case specifically is interesting to study as the planets of the solar system have been shown to roughly lie in a plane [4, 6].

In 2013, Šuvakov and Dmitrašinović [4] made a significant advance by finding twelve new distinct collisionless periodic orbits of three unit masses confined to a plane, presenting a total of fifteen (including three earlier known orbits) in their paper. Since then, hundreds more planar periodic orbits have been discovered [1].

Montgomery, in his paper [2], mapped planar configurations to the shape sphere $S^2 \subset \mathbb{R}^3$. One step involved contracting $S^3 \subset \mathbb{R}^4$ to $S^2$ by way of a Hopf fibration. However, some information about the orbit is lost this way. A promising approach to studying these orbits to rather represent $S^3 - \{(0,0,0,1)\}$ as $\mathbb{R}^3$, therefore preserving information. Motivated by Montgomery's work, we propose a four-step procedure. Concretely, we start with the space of all reduced planar configurations, then:

1. Impose a center-of-mass constraint, reducing dimension by 2.

2. Perform a linear transformation to diagonalize the quadratic form which emerges from the previous mapping.
3. Normalize the surface to $S^3$.
4. Stereographically project $S^3$ onto $\mathbb{R}^3$.

By following a periodic solution in time, the image of these maps becomes a closed curve in $\mathbb{R}^3$ whose knot type can be identified.

In this paper, we described our steps and illustrate their application to the fifteen orbits of Šuvakov and Dmitrašinović. We then provide a table summarizing the orbit classification results. We conclude by highlighting possible future work.

## 2. Assumptions and Constraints

We begin with three point masses of unit mass, indexed $i = 1, 2, 3$ each associated with a position vector $\vec{P} = (x_i, y_i)$ in $\mathbb{R}^2$. Thus, the initial configuration space is $\mathbb{R}^6$. We consider the set of configurations which adhere to the following two constraints.

1. Centre-of-mass constraint:

$$\sum_{i=1}^{3} \vec{P}_i = (0, 0).$$

2. Size constraint:

$$\sum_{i=1}^{3} ||\vec{P}_i||^2 = 1.$$

We call this set *reduced.* Note that we may translate the center-of-mass of any three-body configuration to $(0, 0)$ due to Galilean invariance. Furthermore, any three vectors may be scaled down such that they satisfy the size constraint by redefining the points as the following.

$$\vec{P}'_i = \frac{\vec{P}_i}{\sqrt{\sum_{i=1}^{3} ||\vec{P}_i||^2}}.$$

The set of all such $(\vec{P}_1, \vec{P}_2, \vec{P}_3)$ adhering to both constraints lies on a 4-dimensional surface.

## 3. The Procedure

The four mappings are summarised in the following diagram.

$$\mathbb{R}^6 \to \mathbb{R}^4 \to \mathbb{R}^4 \to S^3 \to \mathbb{R}^3$$

### 3.1. Fixing Center of Mass

Since

$$\sum_{i=1}^{3} \vec{P}_i = (0, 0).$$

we rearrange for $\vec{P}_3$:

$$\vec{P}_3 = -(\vec{P}_1 + \vec{P}_2).$$

As a result, every configuration is determined by $\vec{P}_1$ and $\vec{P}_2$ alone. By the size constraint,

$$||\vec{P}_1||^2 + ||\vec{P}_2||^2 + ||\vec{P}_3||^2 = ||\vec{P}_1||^2 + ||\vec{P}_2||^2 + ||-\vec{P}_1 - \vec{P}_2||^2 = 1.$$

Equivalently,

$$2x_1^2 + 2x_1x_2 + 2x_2^2 + 2y_1^2 + 2y_1y_2 + 2y_2^2 = 1.$$

Hence, this step effectively decreases dimension by two by sending $(\vec{P}_1, \vec{P}_2, \vec{P}_3) \in \mathbb{R}^6$ to $(x_1, y_1, x_2, y_2) \in \mathbb{R}^4$, subject to the above quadratic constraint.

### 3.2. Diagonalizing the Quadratic Form

Set $\vec{X} = (x_1, x_2)$ and $\vec{Y} = (y_1, y_2)$. The previous constraint shows that

$$\vec{X}^T \begin{pmatrix} 2 & 1 \\ 1 & 2 \end{pmatrix} \vec{X} + \vec{Y}^T \begin{pmatrix} 2 & 1 \\ 1 & 2 \end{pmatrix} \vec{Y} = 1.$$

Call the shared $2 \times 2$ matrix $A$. We see that $A$ has eigenvalues $\lambda_1 = 3$ and $\lambda_3 = 1$. To diagonalise, we must find a $\theta$ such that the rotation matrix

$$R(\theta) = \begin{pmatrix} \cos\theta & -\sin\theta \\ \sin\theta & \cos\theta \end{pmatrix}$$

satisfies

$$R(\theta)^T A R(\theta) = \text{diag}(3, 1).$$

By multiplying out the matrices, we see that $\theta = \pi/4$ is valid. Thus,

$$R = R(\tfrac{\pi}{4}) = \frac{1}{\sqrt{2}} \begin{pmatrix} 1 & -1 \\ 1 & 1 \end{pmatrix}.$$

Since $R$ is orthogonal, $R^T = R^{-1}$. Therefore, the new basis vectors are

$$\begin{pmatrix} u_1 \\ u_2 \end{pmatrix} = R^T \begin{pmatrix} x_1 \\ x_2 \end{pmatrix} \text{ and } \begin{pmatrix} v_1 \\ v_2 \end{pmatrix} = R^T \begin{pmatrix} y_1 \\ y_2 \end{pmatrix},$$

which satisfy

$$(u_1 \; u_2) A \begin{pmatrix} u_1 \\ u_2 \end{pmatrix} = 3u_1^2 + u_2^2$$

and

$$(v_1 \; v_2) A \begin{pmatrix} v_1 \\ v_2 \end{pmatrix} = 3v_1^2 + v_2^2.$$

The constraint becomes

$$3u_1^2 + u_2^2 + 3v_1^2 + v_2^2 = 1.$$

Therefore, this step places the configuration on a hyperellipsoid in $\mathbb{R}^4$.

### 3.3. Normalizing onto $S^3$

We perform a change of variables to map the quadruple $(u_1, u_2, v_1, v_2)$ onto $S^3 \subset \mathbb{R}^4$. Define

$$(s_1, s_2, t_1, t_2) = (\sqrt{3}u_1, u_2, \sqrt{3}v_1, v_2).$$

By construction, we have that

$$s_1^2 + s_2^2 + t_1^2 + t_2^2 = 1.$$

Hence, $(s_1, s_2, t_1, t_2)$ must lie on $S^3$.

### 3.4. Stereographic Projection of $S^3 - \{(0,0,0,1)\}$ to $\mathbb{R}^3$

To perform a stereographic projection, we must remove a point, which we choose to be the point $(0,0,0,1) \in S^3$. We can do this because none of the trajectories we concern ourselves with (e.g. the configurations presented in (Šuvakov)) go through $(0,0,0,1)$ and the projection through $(0,0,0,1)$ yields us a simple formula. Of course, we could have picked any arbitrary point to do the projection through.

We project the remainder to $\mathbb{R}^3$. Formally, let

$$(s_1, s_2, t_1, t_2) \in S^3 - \{(0,0,0,1)\}.$$

We define

$$(x, y, z) = \left(\frac{s_1}{1-t_2}, \frac{t_1}{1-t_2}, \frac{s_2}{1-t_2}\right).$$

This yields a bijection from $S^3 - \{(0,0,0,1)\}$ to $\mathbb{R}^3$. Therefore, under the compositions of the four previous steps, each configuration $(\vec{P}_1, \vec{P}_2, \vec{P}_3)$ becomes a closed loop in $\mathbb{R}^3$.

## 4. Closed Loops and Knot Classification

Let $L = (\vec{P}_1(t), \vec{P}_2(t), \vec{P}_3(t))$ be a periodic collisionless planar orbit with period $T > 0$ which adheres to the centre-of-mass condition and the size condition. Represent $L$ as $(x_1, y_1, x_2, y_2)$, as described in (3.1). Under the mappings presented in (3.2), (3.3), and (3.4), we are given a continuous curve

$$C: [0, T] \to \mathbb{R}^3,$$

where

$$C(t) = (IV \circ III \circ II)(x_1, y_1, x_2, y_2),$$

mappings $II$, $III$, and $IV$ represent the mappings outlined in (3.2), (3.3), and (3.4), respectively, and $C(0) = C(T)$. We can now classify $C$ as a knot.

### 4.1 Application to Šuvakov and Dmitrašinović's Orbits

We attempt to classify the trajectories which Šuvakov and Dmitrašinović discovered in [4]. We first numerically approximated each configuration with a Runge-Kutta algorithm with linear step size 0.0001 until a period elapsed. Restriction to one period made error and deviation practically negligible. Subsequently, we translated and scaled the collection or positions to follow the size and center-of-mass constraints before applying the mappings in (3.2), (3.3) and (3.4). To determine knot type, we projected the orbit to an orthogonal unit basis, then applied Reidemeister moves.

Some orbits are easily determinable, such as I.A.2 butterfly II, while others are more difficult, such as I.A.1 butterfly I. Both trajectories are shown in Figure 1. Figure 2 shows how a curve can be simplified using Reidemeister moves.

Figure 1. I.A.2 butterfly II (left) and I.A.1 butterfly I (right). Lighter colours denote higher elevation (when viewed in 3D after Step IV).

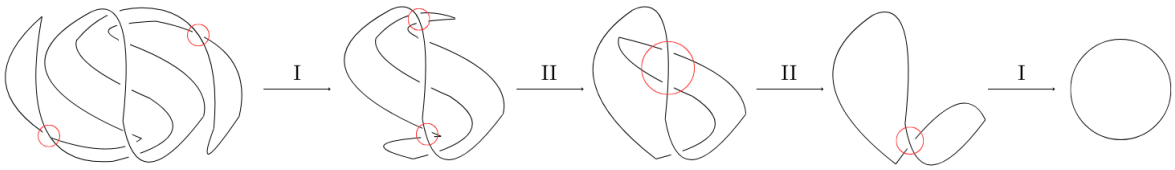


Figure 2. I.A.2 butterfly II being deformed into the unknot. The red circles show the crossings being acted upon. Operations I, II, and III represent their corresponding Reidemeister moves.

The following table summarises our classifications of each orbit. We include the initial velocity parameters, $\dot{x}(0)$, $\dot{y}(0)$, the free group element, as given in [5], and the resulting knot type. We see that class II.C does not have an orbit which is non-trivial—thus, not every class has a non-trivial knot. We also notice that I.A.1 butterfly I and I.A.2 butterfly II have the same free-group element, yet have different knot types, therefore answering both of our questions.

Table 1. Initial conditions of the three-body orbits and knot classification. Labelling for the orbits follow what is written in (Šuvakov 2013). Quantities $\dot{x}_i(0)$ and $\dot{y}_i(0)$ are the $i$th body's initial

| Class, Number and Name | $\dot{x}(0)$ | $\dot{y}(0)$ | Free Group Element | Knot Classification |
|---|---|---|---|---|
| I.A.1 butterfly I | 0.30689 | 0.12551 | $(ab)^2(AB)^2$ | trefoil |
| 1.A.2 butterfly II | 0.39295 | 0.09758 | $(ab)^2(AB)^2$ | unknot |
| I.A.3 bumblebee | 0.18428 | 0.58719 | 1 | unknot |
| I.B.1 moth I | 0.46444 | 0.39606 | $ba(BAB)ab(ABA)$ | figure-eight |
| I.B.2 moth II | 0.43917 | 0.45297 | $(abAB)^2A\ (baBA)^2$ | unknot |
| I.B.3 butterfly III | 0.40592 | 0.23016 | $(ab)^2(ABA)(ba)^2(BAB)$ | unknot |
| I.B.4 moth III | 0.38344 | 0.37736 | $(babABA)^2a(abaBAB)^2b$ | unknot |
| I.B.5 goggles | 0.08330 | 0.12789 | $(ab)^2ABBA(ba)^2BAAB$ | trefoil |
| I.B.6 butterfly IV | 0.350112 | 0.07934 | $((ab)^2(AB)^2)^6A((ba)^2(BA)^2)^6B$ | unknot |
| I.B.7 dragonfly | 0.08058 | 0.58884 | $(b^2(ABabAB))(a^2(BAbaBA))$ | unknot |
| II.B.1 yarn | 0.55906 | 0.34919 | $(babABabaBA)^3$ | trefoil |
| II.C.2a yin-yang I | 0.51394 | 0.30474 | $(ab)^2(ABA)ba(BAB)$ | unknot |
| II.C.2b yin-yang I | 0.28270 | 0.32721 | $(ab)^2(ABA)ba(BAB)$ | unknot |
| II.C.3a yin-yang II | 0.41682 | 0.33033 | $(abaBAB)^3(abaBAbab)(ABAbab)^3(AB)^2$ | unknot |
| II.C.3b yin-yang | 0.41734 | 0.31310 | $(abaBAB)^3(abaBAbab)(ABAbab)^3(AB)^2$ | unknot |

velocities in the $x$ and $y$ direction, respectively. The values $x_i(0)$ and $y_i(0)$ are the $i$th body's positions in the $x$ direction and $y$ direction, respectively. The initial velocities of the bodies are

$\dot{x}_1(0) = \dot{x}_2(0) = \dot{x}(0), \dot{x}_3(0) = -2\dot{x}(0), \dot{y}_1(0) = \dot{y}_2(0) = \dot{y}(0), \dot{y}_3(0) = -2\dot{y}(0)$. The initial positions of the bodies are $x_1(0) = -x_2(0) = -1, x_3(0) = 0, y_1(0) = y_2(0) = y_3(0) = 0$. The gravitational constant $G$ is taken to be 1 and the masses $m_1$, $m_2$, $m_3$ are equal and taken to be 1.

$^1(b(ABab)\text{^}2\ A\text{^}2\ (baBA)\text{^}2\ ba)\ (B\text{^}2\ (abAB)\text{^}2\ a\text{^}2\ (BAba)\text{^}2\ BA)$

## 5. Conclusion

We presented a series of four steps that turn a planar periodic equal-mass three-body system into a closed curve in $\mathbb{R}^3$, whose knot type can then be identified. Afterwards, we applied the mappings to the fifteen trajectories Šuvakov and Dmitrašinović displayed in [5], showing that the majority of the orbits can be classified as the unknot. But, three yield the trefoil knot and another produces the figure-eight, showing that non-trivial knottedness is possible.

Future work could be dedicated to applying the mappings described previously to more periodic orbits, such as the results presented in [1] to see if more complicated knot types emerge or proving that only a certain set of knots are able to appear. Another avenue to consider would be to generalize the mappings to non-identical masses.

## Works Cited

1. Li. X. and S. Liao. ``More Than Six Hundred New Families of Newtonian Periodic Planar Collisionless Three-Body Orbits." *Periódicos da CAPES*, 2017, https://www.periodicos.capes.gov.br/index.php/acervo/buscador.html?task=detalhes&id=W3105606363
2. Montgomery, R. “The N-body Problem, the Braid Group, and Action-Minimizing Periodic Solutions.” *Nonlinearity*, vol. 11, no. 2, 1998, pp. 363–376.
3. Poincaré, H. “Sur le problème des trois corps et les équations de la dynamique.” *Acta Mathematica*, vol. 13, 1890, pp. 1–270. https://doi.org/10.1007/BF02392506.
4. Souami, D., and J. Souchay. “The Solar System’s Invariable Plane.”, vol. 543, A133, 2012. https://doi.org/10.1051/0004-6361/201218903.
5. Šuvakov, M., and V. Dmitrašinović. “Three Classes of Newtonian Three-Body Planar Periodic Orbits.” *Physical Review Letters*, vol. 110, no. 11, 15 Mar. 2013, p. 114301. doi:10.1103/PhysRevLett.110.114301.
6. Xie, J.-W., S. Dong, Z. Zhu, D. Huber, Z. Zheng, P. De Cat, J. Fu, H.-G. Liu, A. Luo, Y. Wu, H. Zhang, H. Zhang, J.-L. Zhou, Z. Cao, Y. Hou, Y. Wang, and Y. Zhang. “Exoplanet Orbital Eccentricities Derived from LAMOST–Kepler Analysis.” *Proceedings of the National Academy of Sciences of the United States of America*, vol. 113, no. 41, 26 Sept. 2016, pp. 11431–11435. doi:10.1073/pnas.1604692113.